J. Plasma Phys. (2025), *vol*. 91, E69
doi:10.1017/S0022377825000169

Intermittency assessed through a model of kurtosis–skewness relation in MHD in fast dynamo regimes

Yannick Ponty[1], Hélène Politano[2] and Annick Pouquet[3]

[1]Université Côte d'Azur, Observatoire de la Côte d'Azur, Laboratoire Lagrange, CNRS, Nice, France
[2]Université Côte d'Azur, Laboratoire JA Dieudonné, CNRS, Nice, France
[3]National Center for Atmospheric Research, PO Box 3000, Boulder, CO 80307, USA

Corresponding author: Yannick Ponty, yannick.ponty@oca.eu

(Received 19 November 2024; revision received 7 February 2025; accepted 11 February 2025)

Intermittency as it occurs in fast dynamos in the magnetohydrodynamics (MHD) framework is evaluated through the examination of relations between normalized moments at third order (skewness S) and fourth order (kurtosis K) for both the velocity and magnetic field, and for their local dissipations. As investigated by several authors in various physical contexts such as fusion plasmas (Krommes 2008 *Phys. Plasmas* **15**, 030703), climate evolution (Sura & Sardeshmukh 2008 *J. Phys. Oceano.* **38**, 639-647), fluid turbulence or rotating stratified flows (Pouquet *et al.* 2023 *Atmosphere* **14**, 01375), approximate parabolic $K(S) \sim S^{\alpha}$ laws emerge whose origin may be related to the applicability of intermittency models to their dynamics. The results analyzed herein are obtained through direct numerical simulations of MHD flows for both Taylor–Green and Arnold–Beltrami–Childress forcing at moderate Reynolds numbers, and for up to 3.14×10^5 turn-over times. We observe for the dissipation $0.2 \lesssim \alpha \lesssim 3.0$, an evaluation that varies with the field, the forcing and when filtering for high-skewness intermittent structures. When using the She & Lévêque (1994) *Phys. Rev. Lett.* **72**, 336-339 intermittency model, one can compute α analytically; we then find $\alpha \approx 2.5$, clearly differing from a (strict) parabolic scaling, a result consistent with the numerical data.

Keywords: MHD, Fast dynamo, Intermittency, Kurtosis, Dissipation, Turbulence

1. Introduction

One striking property of turbulent flows is their lack of predictability, as well as their intermittency, associated with the presence of intense and isolated patterns at small scales, such as vortex filaments and current sheets, or coherent structures at large scale. Such extreme events can be assessed through their probability distribution functions (PDFs), and thus through their normalized moments such as the

skewness and kurtosis (definitions are given in § 2). These intense structures have been identified in many experiments, observations and direct numerical simulations (see for recent reviews e.g. Matthaeus *et al.* 2015; Yeung, Zhai & Sreenivasan 2015; Chen 2016; Camporeale *et al.* 2018; Ergun 2020; Schekochihin 2022). The ensuing dissipation is found in a reduced volume of the system, in both neutral fluids (Bradshaw, Farhat & Grujic 2019; Rafner *et al.* 2021; Buaria, Pumir & Bodenschatz 2022) and magnetohydrodynamics (MHD) (see e.g. Politano, Pouquet & Sulem 1995; Meneguzzi *et al.* 1996; Mallet, Schekochihin & Chandran 2017; Zhdankin, Boldyrev & Mason 2017; Adhikari *et al.* 2020). This physical intermittency volume can be in fact smaller than for fully developed turbulence, as shown explicitly in the presence of gravity waves (Marino *et al.* 2022). It is also found in the ocean (van Haren *et al.* 2016), as well as in clear air turbulence, the origin of which remains rather ill understood although Kelvin–Helmholtz and shear instabilities are likely to be the culprit (Imazio *et al.* 2023), as for the other examples given here. Similar observations are documented for plasma disruptions.

Intermittency can be characterized in many ways, such as when evaluating anomalous exponents of structure functions. Perhaps more directly, one can assess when and where normalized third- and fourth-order moments, skewness S and kurtosis K, differ from their Gaussian values. There is a long history of such measurements; for example, both skewness and kurtosis have been used to map a flow, such as in meandering jets in the ocean (Hughes, Thompson & Wilson 2010), or in climate data reanalysis (Petoukhov *et al.* 2008).

One way to condense the data further is to look for $K(S)$ relations, often found to be close to parabolic in a variety of contexts (see Pouquet *et al.* 2023 and references therein for a recent review), e.g. for the Navier–Stokes (NS) equations, in the presence or not of stratification and/or rotation, as relevant to the atmosphere, the ocean and climate (Lenschow, Mann & Kristensen 1994; Sura & Sardeshmukh 2008). Such quasi-parabolic laws were also found in laboratory and astrophysical plasmas (see for example Labit *et al.* 2007; Krommes 2008; Sattin *et al.* 2009; Garcia 2012; Guszejnov *et al.* 2013; Mezaoui, Hamza & Jayachandran 2014; Furno *et al.* 2015; Miranda *et al.* 2018). More recently, Sladkomedova *et al.* (2023) analyzed the intermittency of the density in MAST (Mega Ampere Spherical Tokamak) plasmas, and found that the data agrees with the $K(S)$ model given by Garcia (2012) (see also Guszejnov *et al.* 2013; Losada, Theodorsen & Garcia 2023).[1]

Detailed knowledge of intermittency in plasmas and turbulent systems in general may lead to a better understanding of their PDFs and of the dissipation mechanisms at play. It is in this context that we want to examine in this paper the intermittent properties of MHD through the possible relationship between excess kurtosis and skewness for the velocity and magnetic field, as well as for their local dissipation. MHD has, of course, many different regimes, and we concentrate here on one subset, namely that of the fast dynamo in its nonlinear phase and at moderate Reynolds number for which long runs are available, up to in excess of $10^5\tau_{nl}$, where

$$\tau_{nl} = L_{int}/V_{rms} \tag{1.1}$$

is the turn-over time of the turbulence based on the large-scale velocity V_{rms} and on the integral length scale L_{int}. In the next section are written the equations and definitions needed for our analysis of numerical MHD data for a fast dynamo regime,

[1]The model is based on moments up to fourth order as well as on an estimate of the number of the intermittent events that are observed simultaneously.

as well as information on the direct numerical simulations (DNSs) employed herein. In § 3, we analyze the numerical results, and in § 4 we give an interpretation of them within a specific model of intermittency. The last section presents a discussion and our conclusions.

2. Equations and numerical set-up

2.1. *Equations and definitions*

The equations for MHD in the incompressible case are written as usual as

$$[\partial_t + \boldsymbol{u}\cdot\nabla]\boldsymbol{u} \equiv D_t\boldsymbol{u} = -\nabla P^\star + \boldsymbol{b}\cdot\nabla\boldsymbol{b} + \nu\Delta\boldsymbol{u} + \boldsymbol{F}_V, \tag{2.1}$$

$$[\partial_t + \boldsymbol{u}\cdot\nabla]\boldsymbol{b} \equiv D_t\boldsymbol{b} = \boldsymbol{b}\cdot\nabla\boldsymbol{u} + \eta\Delta\boldsymbol{b}, \tag{2.2}$$

together with $\nabla\cdot\boldsymbol{u} = 0$, $\nabla\cdot\boldsymbol{b} = 0$; here, $\boldsymbol{u}$, $\boldsymbol{b}$ are the velocity and magnetic field (in Alfvén velocity units), $P^\star$ is the total pressure, ν, η are the viscosity and magnetic diffusivity and $\boldsymbol{F}_V$ is a forcing term. We will use in this paper two types of forcing. The first one is the ABC (Arnold–Beltrami–Childress) forcing, which is a superposition of Beltrami vortices and thus fully helical; it is defined as

$$\boldsymbol{f}_{\mathrm{ABC}} = [\cos y + \sin z]\,\hat{\boldsymbol{x}} + [\sin x + \cos z]\,\hat{\boldsymbol{y}} + [\cos x + \sin y]\,\hat{\boldsymbol{z}}. \tag{2.3}$$

The ABC flow is an eigenfunction of the curl, and it is an exact solution of the Euler equations; thus, for large enough viscosity, it is stable but turbulence develops as the Reynolds number R_V increases. We also take the Taylor–Green (TG) forcing written as

$$\boldsymbol{f}_{\mathrm{TG}} = f_0^{tg}\left\{[\sin x\ \cos y\ \cos z]\,\hat{\boldsymbol{x}} - [\cos x\ \sin y\ \cos z]\,\hat{\boldsymbol{y}} + 0\,\hat{\boldsymbol{z}}\right\}, \tag{2.4}$$

with $f_0^{tg} = 3$. This forcing is globally non-helical, but it can be viewed in fact as an assembly of helical patches of both signs and varied intensities.

We solved numerically our MHD system in a fully periodic box using a classic pseudo-spectral solver, involving a 2/3 dealiasing technique with a parallel CPU-MPI code (CUBBY; Ponty *et al.* 2005). With these two forcings, we compute four simulations altogether, for up to hundreds of thousands of eddy turn-over times, and we record the same number of snapshots for the three-dimensional field components for **v** and **b**. Some of the data and a few of the statistical properties of these runs are given in table 1.

2.2. *Brief description of the runs*

The dynamo problem, concerning the generation of magnetic fields at both large and small scales, is a long-standing topic (see Brandenburg & Subramanian 2005; Rincon 2019 for thorough recent reviews). In the context of this paper, we analyze four simulation runs, focusing on the turbulent dynamo regime. In these simulations, the (fast) dynamo is triggered when the magnetic Reynolds number R_M exceeds a threshold that depends on the magnetic Prandtl number $P_m = \nu/\eta$ (Ponty *et al.* 2005), as seen in run TG3. Sub-critical dynamos can also be observed, where magnetically induced changes to the velocity field play a role, such as in run TG1, which

Run –	n_p	ν	R_V	R_λ	R_N	T_{max}	τ_{nl}	R_M	P_m	r
TG1 –	64	0.07	65.5	25.5	2.98	50×10^3	2.23	111	0.7	1.05
TG3 –	64	0.1	60.	24.3	3.35	130×10^3	1.86	430	3.3	5.26
ABC1 –	64	0.16	210.	45.8	2.4	60×10^3	1.14	32	1.45	1.18
ABC2 –	64	0.2	175.	41.	1.4	314.254×10^3	1.12	21	1.42	1.21

TABLE 1. Characteristics of the runs, with the linear resolution n_p of the cubic grid, ν the viscosity, the Reynolds number $R_V = L_{int} V_{rms}/\nu$ and Taylor Reynolds number $R_\lambda = \lambda V_{rms}/\nu$; $R_N = \eta_\nu n_p/3$ is the so-called Kaneda criterion based on the resolution in terms of the Kolmogorov dissipation length η_ν. TG denotes Taylor– Green runs, and ABC denotes ABC runs (see text). For each run, T_{max} is its total duration, with τ_{nl} in these units between 1 and 2. For the magnetic variables, we give the magnetic Reynolds number $R_M = L_{int} V_{rms}/\eta$, the magnetic Prandtl number $P_m = \nu/\eta$ and $r = R_M/R_M^C$ is the ratio of the magnetic Reynolds number to the (approximate) critical value for the threshold of the dynamo. All these non-dimensional numbers need different definition of scales, like the integral scale $L_{int} = 2\pi \sum E(k)/k/\sum E(k)$ defined using the isotropic energy spectrum computed along the simulation at each wavenumber k, the Taylor scale $\lambda = \sqrt{10}\eta_\nu R_V^{1/4} = \sqrt{10} L_{int} R_V^{-1/2}$ in the inertial range and the Kolmogorov scale $\eta_\nu = [\frac{\epsilon_\nu}{\nu^3}]^{-1/4} = L_{int} R_V^{-3/4}$ at the onset of the dissipation range. We need also one characteristic velocity which is usually taken as the root mean square of the kinetic energy $V_{rms} = \sqrt{2 \sum E(k)}$. The nonlinear time is taken as $\tau_{nl} = L_{int}/V_{rms}$. All the scales and velocity are averaged in time as the simulations develop.

is close to the onset of dynamo action, and living on the sub-critical branch (Ponty *et al.* 2007). It is also worth noting that the Lorenz force's feedback on the velocity field can influence the so-called 'on–off' intermittency of the dynamo, as explored in detail by Alexakis & Ponty (2008) in the context of the ABC runs ABC1 and ABC2. These runs are notable for their short off phases, during which the magnetic field becomes weak enough to revert the system to a hydrodynamic state. The dynamo comes back quickly, with a return to an MHD equilibrium (see figure 1 below). We thus finally have two different types of dynamo turbulence, with a large amount of fluctuations which are analyzed in the next sections, examining the behavior of the third- and fourth-order normalized moment statistics using the full-space temporal field data.

2.2.3. Analysis of the results

3.1. *Field gradient tensors, skewness and kurtosis*

Concerning the data points for measurements, which must be statistically independent, they are taken approximately every τ_{nl}; we recall that measurement errors go as $\sqrt{6/N_s}$, with N_s the number of independent data points (see e.g. Sura & Sardeshmukh 2008). Large samples are needed also because a parabolic fit is quite sensitive to extreme values. Note that it is shown in (Wan *et al.* 2010), in the context of two-dimensional (2-D) MHD turbulence, that an estimate of the kurtosis at small scales requires, in the framework of the DNSs analyzed in that paper, that the (Kolmogorov) dissipation scale be at least twice as large as the cutoff $k_{max} = n_p/3$; this condition is well fulfilled by the runs of table 1 (see parameter R_N).

We analyze the data using the point-wise rates of dissipation of the kinetic and magnetic energy, $\epsilon_v(\boldsymbol{x})$, $\epsilon_m(\boldsymbol{x})$. They are expressed in terms of the symmetric part of

the velocity gradient tensor, namely the strain tensor S^v_{ij}

$$S^v_{ij}(\boldsymbol{x}) = \frac{\partial_j u_i(\boldsymbol{x}) + \partial_i u_j(\boldsymbol{x})}{2}; \quad \epsilon_v(\boldsymbol{x}) = 2\nu \Sigma_{ij} S^v_{ij}(\boldsymbol{x}) S^v_{ij}(\boldsymbol{x}) \tag{3.1}$$

and of the magnetic current density, *viz.* $\epsilon_m(\boldsymbol{x}) = \eta \boldsymbol{j}^2(\boldsymbol{x})$. For completeness, we also define the symmetric part of the magnetic field gradient tensor, namely

$$S^m_{ij}(\boldsymbol{x}) = \frac{\partial_j b_i(\boldsymbol{x}) + \partial_i b_j(\boldsymbol{x})}{2}; \quad \sigma_m(\boldsymbol{x}) = \Sigma_{ij} S^m_{ij}(\boldsymbol{x}) S^m_{ij}(\boldsymbol{x}). \tag{3.2}$$

Note that S^m_{ij} is a pseudo (axial) tensor. The standard expressions for the integrated (space-averaged) kinetic, magnetic and total energy dissipation rates, can respectively be written also as

$$\epsilon_V = \nu \langle |\boldsymbol{\omega}|^2 \rangle; \quad \epsilon_M = \eta \langle |\boldsymbol{j}^2| \rangle \ \epsilon_T = \epsilon_V + \epsilon_M \tag{3.3}$$

with $\boldsymbol{\omega} = \nabla \times \boldsymbol{u}$ the vorticity. Finally, the skewness and excess kurtosis are written below for a scalar field f, with $S_f = 0$, $K_f = 0$ for a Gaussian distribution, with the kurtosis (or flatness) being defined as $F_f = K_f + 3$

$$S_f = \langle f^3 \rangle / \langle f^2 \rangle^{3/2}, \ K_f = \langle f^4 \rangle / \langle f^2 \rangle^2 - 3. \tag{3.4}$$

3.2. *Some models for $K(S)$ relations*

A $K(S)$ parabolic law has been derived explicitly in Sura & Sardeshmukh (2008) for a model of oceanic sea-surface temperature anomalies, based on the dynamics of a specific linear Langevin model with both additive and multiplicative noises. Analyzing the corresponding Fokker–Planck equation for the stationary PDF, these authors can show analytically that, in the limit of weak multiplicative noise, one has $K(S) = 3S^2/2$. Multiple other studies show the plausibility of a Langevin model for parabolic $K(S)$ behaviors in different contexts as exemplified e.g. in Hasselmann (1962) and Sattin *et al.* (2009) (see also Pouquet *et al.* (2025) for nonlinear Langevin models). Note that, in a Langevin equation, in a sense, one is getting rid of the closure problem for turbulent motions since it is linear, with the complex nonlinear small-scale dynamics bundled up in a rapid stochastic forcing with an assumption of (mostly) local interactions among these fast motions.

In fact, models in the framework of fusion plasmas have also been written, for example in the context of magnetically confined experiments. In Garcia (2012), the dynamics, as for dissipation events, is viewed as a random sequence of bursts as opposed to a quasi-continuum. These bursts are occurring independently and following a Poisson process. When taking for the shape of these bursts a sharp rise and a slow exponential decay, one can compute $K(S)$ relations which, for an exponential distribution of burst amplitudes, becomes $K(S) = 3/2(S^2 - 1)$.

3.3. *Collecting the spatio-temporal data for further analysis*

Our methodology is the following. For each field variable at a fixed observation time T_O, as for the vertical component of the velocity $v_z(\boldsymbol{x}, T_O)$, or the magnetic energy dissipation $\eta \boldsymbol{j}^2(\boldsymbol{x}, T_O)$, the data are collected roughly every turn-over time τ_{nl}, for in excess of 5×10^4 outputs, as shown in column T_{max} in table 1. For each full-cube temporal data output at T_O the spatially dependent 3-D fields we analyze are computed point-wise at each $\boldsymbol{x}$ location in the n_p^3 data cube. The PDFs are

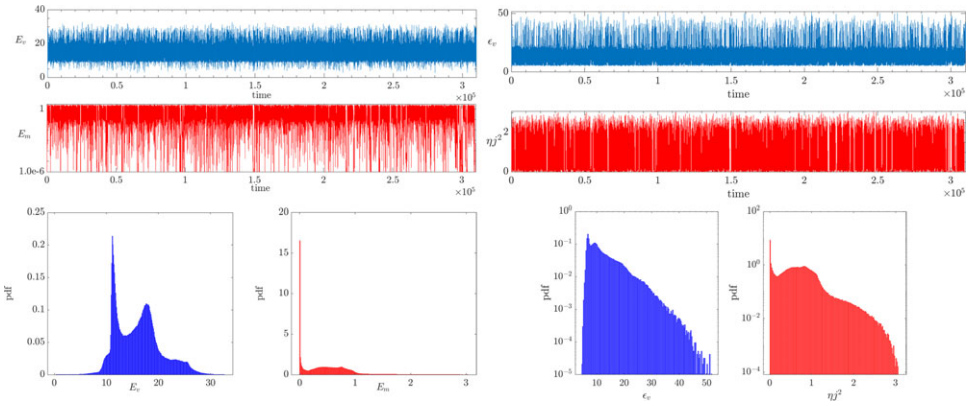

FIGURE 1. Run ABC2: temporal evolutions, with kinetic variables in blue and magnetic ones in red. Top, left and right: kinetic energy and its dissipation, ϵ_v. Middle, left and right: magnetic energy and its dissipation, $\epsilon_m = \eta\langle \boldsymbol{j}^2 \rangle$. Note the different units on axes, and the lin–log scale for magnetic energy. Bottom: probability density functions of the kinetic and magnetic energies (two left plots), and of their dissipation (two right plots), with lin–log plots used for the latter.

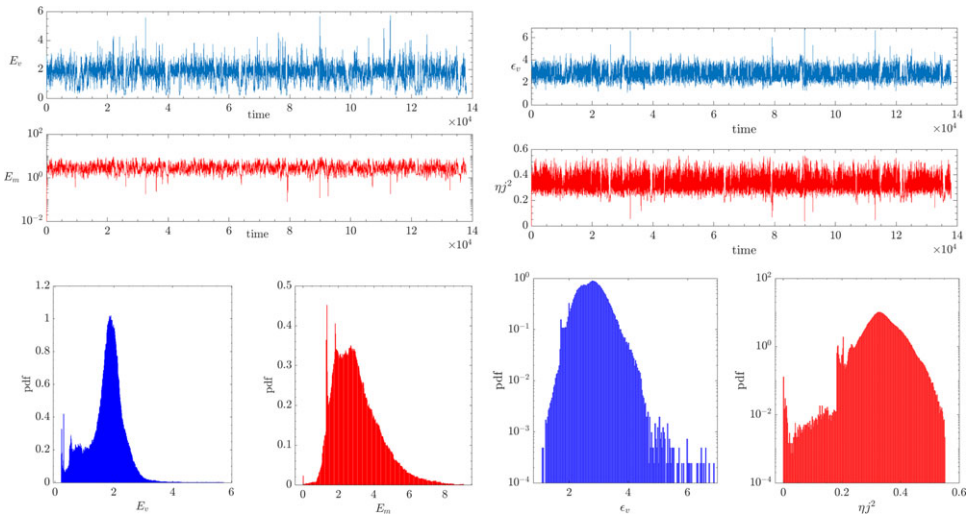

FIGURE 2. Similar plots as in figure 1 but now for the TG3 run.

constructed for these various fields, at that fixed time T_O, and their second, third and fourth moments are evaluated to yield skewness and kurtosis for that time index T_O. These data are then assembled in $K(S)$ plots for the different physical variables of interest. In figures 3 and 4, the time arrow of the data is indicated by the color of the points in the scatter plots, with a rainbow code as given by the color bar at the left of the plots, with purple at early times and red at late times. We note that, having in excess of 5×10^4 time stamps $T_O^{(i)}$ for all runs, the error on the skewness is less than 0.025, and twice that for the kurtosis. As expected, these systems achieve statistical equilibria rapidly, in a few τ_{nl} (see figures 1 and 2 giving the whole time span of the runs for the kinetic and magnetic energies).

Note that this methodology does not correspond to a spatial analysis of intermittency at a fixed time, such as the first maximum of dissipation, given the moderate spatial resolution of the runs analyzed herein. This would lead to a study of the localization and intensity of extreme events at that time, but this is not the purpose of this study. Rather, we instead consider solely here the statistical variations over long times of the spatial intermittency of several field statistics in a global way. We do that in terms of overall variation of non-dimensionalized moments of various functionals of the velocity and magnetic fields as they evolve in time. With samples taken roughly every turn-over time, the statistical data points can be considered as independent. This leads to an investigation of the scatter in values of both K and S for a sample of field functionals, and thus of the $K(S)$ relationships that may emerge for them, with each point on the scatter plots of figures 3 and 4 corresponding to a given T_O. We finally note that these analyses require substantial storage capabilities even at moderate spatial resolutions, so that the various statistical variables of interest and their moments are better computed *a priori*, and stored as the runs progress.

3.4. *Overall data analysis*

We give for the ABC2 flow (figure 1) and for the TG3 case (figure 2) the temporal evolution of the kinetic (top) and magnetic (middle) energy as a function of time on the left, and on the right of their respective total dissipations, $\epsilon_{V,M}$. Note that time is expressed in output counts, with a turn-over time being roughly twice that. At the bottom are given the energy PDFs for the velocity (blue, leftmost) and the magnetic field (red, rightmost plots.) In all cases, there are sustained fluctuations in the amplitude of the fields, and in the case of the ABC run, lapses in both kinetic and magnetic energy corresponding to the on–off mechanism. This is directly related to the fact that the PDFs, in that case, have two relative maxima (with one peak close to zero for the magnetic field), whereas in the case of the TG forcing, the structure of the PDFs is closer to being unimodal. We note that exponential fits in the case of the dissipation fields are plausible, but not yet very strongly marked given the moderate range of Reynolds numbers in these runs.

Figure 3 gives $K(S)$ for various fields; at top, we display the $K(S)$ relationship for the z-component of the velocity, the square vorticity and the kinetic energy dissipation, namely $K_{v_z}(\boldsymbol{x})$, $K_{\omega^2}(\boldsymbol{x})$ and $K_{\epsilon_v}(\boldsymbol{x})$. At bottom we plot the equivalent fields for the magnetic induction, namely $K_{b_z}(\boldsymbol{x})$, $K_{\sigma_m}(\boldsymbol{x})$ and $K_{\eta j^2}(\boldsymbol{x})$. The blue lines correspond to $K = [3/2][S^2 - 1]$ as mentioned before (see § 3.2).

We note the following: whereas for NS turbulence, the three components of the velocity field are Gaussian with the $K(S)$ relation centered on the (0, 0) point, here, the peak in values for K at $S \approx 0$ for v_z is up to $K \approx 14$, and rather narrowly centered around $S_{v_z} \approx 0$; high K values are also present for b_z. The hydrodynamic case analyzed in Pouquet *et al.* (2023) is computed at comparable R_λ and n_p (but not T_{max}), and both S and K for the velocity are close to 0. On the other hand, for stratified flows with or without rotation, the vertical component of the velocity, v_z, can have high kurtosis and high values itself; this is associated with the intermittency of dissipation because of the variability of the system dominated by waves with the sudden development of small dissipative scales through shear-related instabilities. For this MHD run, the x and y components of the velocity behave approximately in the same way as v_z (not shown), with a skewness comparable to that of v_z but smaller kurtosis.

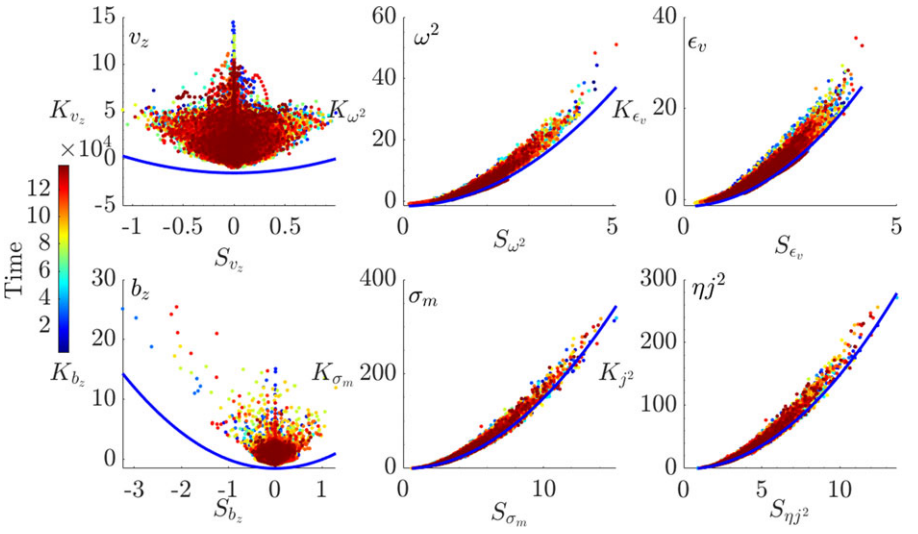

FIGURE 3. Top: for run TG3, $K(S)$ for the vertical velocity v_z (left), the square vorticity density $\boldsymbol{\omega}^2$ (middle) and the point-wise kinetic energy dissipation ϵ_v (right). Bottom: $K(S)$ for b_z (left), σ_m (middle) and $\eta \boldsymbol{j}^2$ (right). The color bar at left indicates the temporal clock in units of turn-over times, with early (late) times in blue (red). The blue lines follow $K(S) = 3/2[S^2 - 1]$.

The symmetric and anti-symmetric parts of both the velocity and magnetic field gradient tensors have both high skewness and high kurtosis and for them, a quasi-parabolic fit is appropriate. The magnetic dissipation has higher kurtosis and thus is likely significantly more intermittent than its kinetic counterpart, and similarly for σ_m and vorticity. On the other hand, both kinetic and magnetic dissipations have lower skewness and kurtosis than for the other part of their gradient tensors, although their statistics overall are similar. We recall that double exponential (Laplace), or Weibull distributions have small S of either sign and high kurtosis (Bertin & Clusel (2006); Biri, Scharffenberg & Stammer 2015; 2016). In that context, we note that it is shown in Sorriso-Valvo *et al.* (2018) that a proxy of energy transfer for the solar wind can be defined based on exact laws for MHD corresponding to the conservation of energy and cross-helicity $H_C = \langle \boldsymbol{v} \cdot \boldsymbol{b} \rangle$; these proxy fields display high intermittency in Helios 2 (and Ulysses) data, with plausible stretched exponential fits. A final remark is that data points with $[K, S] \approx 0$ must be dominated by random noise at these times; they could correspond to relaxation intervals following sharp bursts in energy dissipation.

We now check whether this behavior is observed as well for another type of forcing. In figure 4 are plotted the $K(S)$ relationships at the top for v_z (left), $\boldsymbol{\omega}^2$ (middle) and ϵ_v (right) and (middle row), b_z (left), σ_m (middle) and $\eta \boldsymbol{j}^2$ (right), as in figure 3 but now for run ABC2 with a fully helical ABC forcing. Values for (S, K) for both runs are comparable except for the vertical component of the velocity due to its specific structure. We added in the last row of figure 4 the $K(S)$ plots for the magnetic energy (left) and σ_m (right) for the same run, and using now log–log coordinates. Power laws are conspicuous above some threshold in skewness, with $E_m \approx 0.96 S^{2.20}$, $\sigma_m \approx 0.96 S^{2.25}$, $\eta j^2 \approx 1.05 S^{2.17}$.

Finally, due to the strong symmetries of the initial conditions and forcing of the dynamos analyzed in this paper, one could wonder whether the addition of a small noise would change the results. On the other hand, in view of the length of the

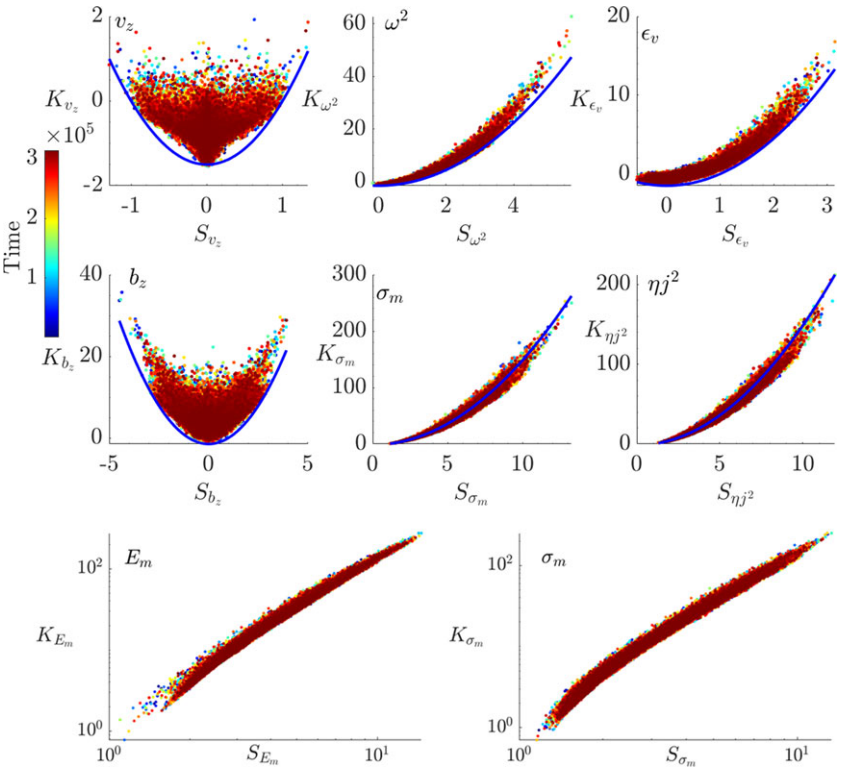

FIGURE 4. The first two rows are the same as figure 3 for run ABC2 with $R_V \approx 175$ and $T_{max} \approx 3.14 \times 10^5$. Bottom: $K(S)$ is plotted for the magnetic energy E_m (left) and for the symmetric part of the magnetic field gradient tensor σ_m (right), using now log–log coordinates. Approximate fits give for both $\alpha \approx 2.2$, $\kappa \approx 1.0$.

computations, well beyond what can be estimated for a reasonable Lyapounov time of separation of trajectories, it is unlikely that the overall results, and in particular the quasi-parabolic law for dissipation, would be altered. Indeed, one can find estimates of the first Lyapounov exponent λ_1, in the ABC dynamo for example, with $\lambda_1 \sim 0.073$ for a run with $R_V \approx 60$, $P_M = 4$, comparable to what we have here (Zienicke, Politano & Pouquet 1998; Alexakis & Ponty 2008), meaning that, after roughly $14\tau_{nl}$, the initial conditions have been forgotten.

4. Kurtosis–skewness law as given by classical intermittency models

We can in fact compute the scaling exponent α_f in the relationship $K(S) \sim S^{\alpha_f}$, assuming the usual formulation for the structure functions of order p for a scalar field f, namely the field differences over a distance r, $\langle \delta f(r)^p \rangle \sim r^{\zeta_p}$; one obtains for α_f

$$\alpha_f = \frac{\zeta_4 - 2\zeta_2}{\zeta_3 - \frac{3}{2}\zeta_2}. \tag{4.1}$$

Within the framework of the standard multi-fractal She & Lévêque (1994) (SL) model for fluids (indicated by the index slf), and generalized for MHD in Grauer,

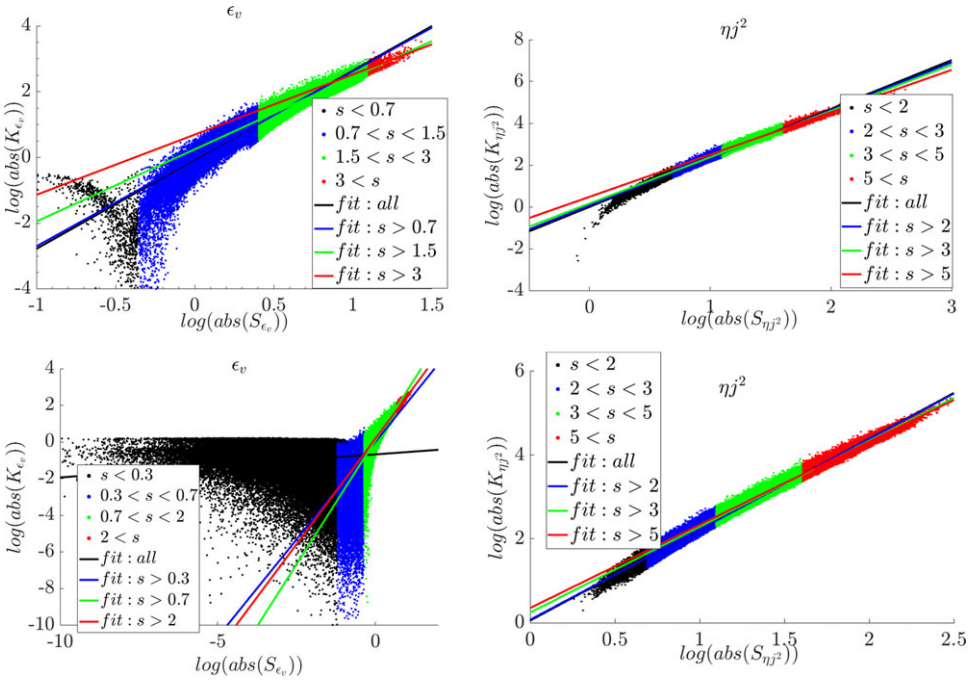

FIGURE 5. Log–log plot for $|K|(|S|) = \kappa |S|^{\alpha}$, runs TG3 (top) and ABC2 (bottom), for kinetic (left) and magnetic (right) dissipation. Thresholds in S are displayed in different colors, and similarly for the power-law fits, as indicated in each inset.

Krug & Mariani (1994) and Politano & Pouquet (1995) (index slm), one has

$$\zeta_p^{slf} = \frac{p}{9} + 2\left[1 - \left(\frac{2}{3}\right)^{p/3}\right] \; ; \; \alpha_{slf} = \frac{2[1 - 2(2/3)^{2/3} + (2/3)^{4/3}]}{7/3 - 3(2/3)^{2/3}} \approx 2.56 \; ; \quad (4.2)$$

$$\zeta_p^{slm} = \frac{p}{8} + 1 - \left(\frac{1}{2}\right)^{p/4} \; ; \; \alpha_{slm} = \frac{3 - 4(1/2)^{1/2}}{1 + 2(1/2)^{3/4} - 3(1/2)^{1/2}} \approx 2.53. \quad (4.3)$$

In building these SL models for fluid turbulence (slf) and MHD (slm), an assumption is made that a hierarchy of flux structures exists compatible with a Kolmogorov transfer time scale and with vortex filaments (or in MHD, an isotropic Iroshnikov–Kraichnan wave–eddy interaction and current sheets). This leads to a specific nonlinear relation in p for the ζ_ps. Note that a parabolic scaling, $\alpha = 2$ is obtained when considering the generalized versions of these log-Poisson models – derived in Politano & Pouquet (1995) both for fluids and for MHD – as the intermittency becomes maximal with extreme flux structures whose geometrical signature disappears in the expression of α (see Pouquet *et al.* 2025).

In this context, we compute power-law fits, $|K| = \kappa |S|^{\alpha}$, (as displayed in figures 5 and 6) for the TG3 and ABC2 runs for the kinetic and magnetic dissipations, and for both full and thresholded data. There are clear variations of α with the strength of the intermittency as evaluated through the level of the skewness. Specifically, the chosen thresholds are $S < 2$ (black), $2 \leqslant S < 3$ (blue), $3 \leqslant S < 5$ (green) and $S \geqslant 5$

(red). Power-law fits in these intervals are given using the same colors. The high S, K values reached here are related to the very long integration times allowing for a thorough exploration of configuration space. We note that the velocity field has a broad range with non-intermittent values (black dots) in the sense that both S and K are quite low; it also undergoes a change of sign of the skewness at low values for TG3. We also observe that S and K can be substantially higher for ηj^2 than for the point-wise kinetic energy dissipation, and with less scatter for K at a given S. This difference might be related to the dynamo that controls the behavior of the magnetic field and its dissipation, whereas the velocity, at these resolutions, still feels the effect of the forcing, but the fit that includes these low-S points does not represent the behavior of the more intermittent data.

Skewness and excess kurtosis can be negative, which is why absolute values are used to visualize the realizations. It is important to mention that Fisher's definition is applied here (where a normal distribution corresponds to zero), then negative values (above -3) are common. For magnetic field quantities, the percentage of negative skewness (S) or kurtosis (K) is nearly zero. In contrast, the skewness of the velocity dissipation rate ϵ_v can reach up to 2 % negative values across all realizations (thus represent only few black points in figure 5). Only in the ABC2 case, the proportion of negative and positive kurtosis values of the velocity dissipation becomes equivalent.

We give some more quantitative information in figure 6, looking at variations with threshold in skewness of the power-law index α for the dissipation fields, namely ηj^2 (left) and ϵ_v (right) for the two ABC runs (top) and the two TG runs (bottom); these runs are identified in the inserts by line and color.

We note first that the run TG3 has a higher R_M, and the two ABC runs have higher R_λ. We also note that the overall ranges of variations for the power-law index is lesser for the TG runs than for the ABC runs, probably due to the fact that the TG run is more developed, and the effect of the forcing is lesser. The power-law index for ϵ_v for run ABC2 has a substantially larger range of variation than for ηj^2, with $0^+ < \alpha_{\epsilon_v} \lesssim 5.0$ overall, versus $1.95 < \alpha_{j^2} \lesssim 2.17$. In general, rather abrupt changes in the values of α (and κ, not shown) occur for $S \gtrapprox 0.5$, i.e. when turbulent motions develop locally. For the current, $\alpha_{\eta j^2}$ decreases systematically towards $\alpha_{\eta j^2} \approx 2$ when the threshold in $S_{\eta j^2}$ is increased. We also note that we see a systematic decreasing trend in α towards a value of 2 or slightly lower, a value that can be recovered with the extension of the SL model to more varied dissipative structures (Pouquet *et al.* (2025)). Finally, the constant κ (not shown) is of order unity in all cases, and slightly increases with threshold as long as enough data are available. We also note its quasi-constancy at lower S values.

A common feature of all these plots is that there are notable variations with threshold in S, starting rather abruptly in the case of the ABC flows. This could indicate an effect on the velocity of the influence of the forcing at these moderate Reynolds numbers and that the velocity is not necessarily changed by the magnetic field which remains somewhat weak (see figures 1 and 2 and table 1). Indeed, with the ratio $r = R_M/R_M^C \approx 1^+$ for all runs except run TG3 (see table 1), we are still rather close to the threshold of the onset of the dynamo.

4.5. Discussion, conclusion and perspectives

We have found in this paper that, rather close to the threshold of the fast dynamo regime, a now classical quasi-parabolic behavior between kurtosis and skewness is

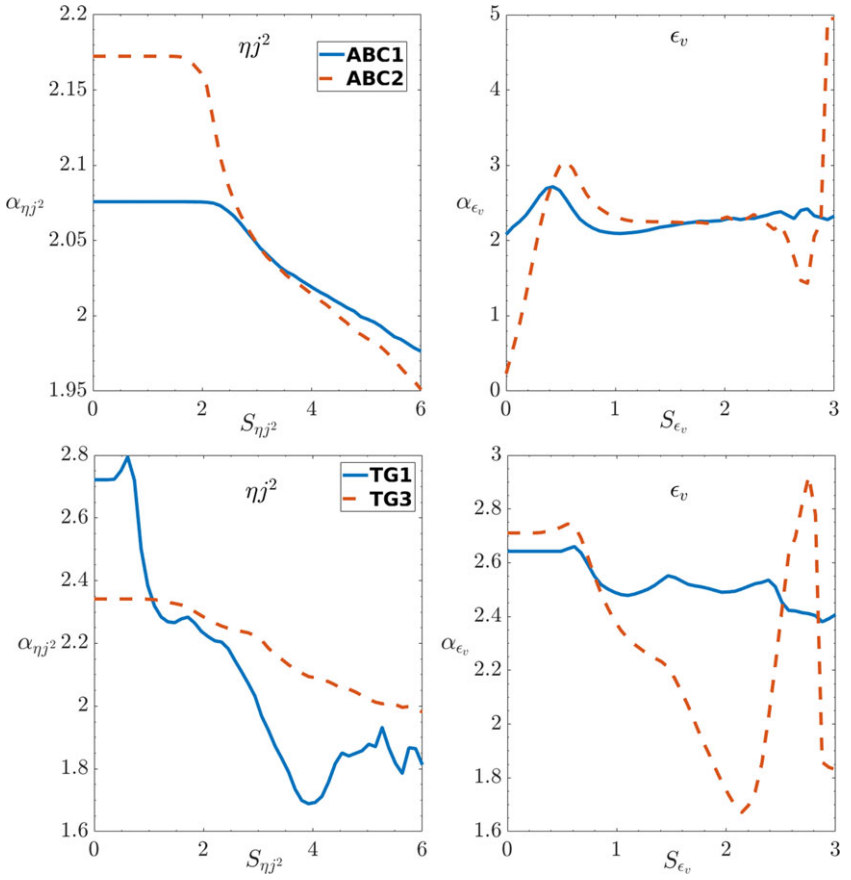

FIGURE 6. The $|K(S)| \sim \kappa |S|^{\alpha}$ fit: variations with filter threshold in S of α for ηj^2 (left) and ϵ_V (right) for the ABC (top) and TG (bottom) flows; runs are differentiated by their colored lines.

present for kinetic and magnetic variables. The numerical data we analyzed represent but one aspect of the study of intermittency in the dynamo regime, and many questions remain. One issue concerns the effect a fully turbulent velocity will have on $K(S)$ scaling and the turbulence of the magnetic field itself. For example, using wavelets, Camporeale *et al.* (2018) could estimate in high-resolution 2-D DNS of Hall-MHD that only 25 % of the volume supports 50 % of the energy transfer, giving thus a quantitative estimate of the intermittency of energy dissipation; we note that, for stratified fluids, this proportion can go as low as 11 % of the kinetic energy dissipation for high kurtosis of the vertical velocity (Marino *et al.* 2022). It will be of interest to examine as well these statistics in the case of fast dynamos at higher Reynolds numbers.

Another question is whether the intermittency of the early dissipation range dominates the statistics, at least at moderate Reynolds numbers. Indeed, one could argue that the intermittency of the dissipation is mostly located in the beginning of the range, due to the ensuing fast decay. In Wu *et al.* (2023), a near-dissipation range intermittency is examined using solar wind data obtained with the Parker Solar Probe. The authors conclude that they find evidence for log-Poisson scaling as modeled for MHD in Grauer *et al.* (1994); Politano & Pouquet (1995), and that such

structures are also almost entirely responsible for the intermittency anisotropy (see also Bian & Li 2024). This may be consistent with stating, as developed already in Kraichnan (1967), that most of the intermittency is in fact at the beginning of the dissipative range.

Another issue is whether or not there is a dynamical consequence of $K(S)$ being close to its Cauchy–Schwarz limit. These inequalities linking K and S can be viewed as a limitation both on skewness (which has to be smaller than some value) and kurtosis, which cannot be too small. It shows that non-Gaussianity and intermittency are unavoidable (except for the trivial ($K = 0, S = 0$) solution), but also that intermittency is limited in the sense that K and S are not independent, and at least for the NS case, the skewness is constrained by the exact law stemming from energy conservation (Kolmogorov 1941), the laws in MHD involving cross-correlations (see for a recent review Marino & Sorriso-Valvo 2023). Furthermore, as noted by several authors, $K(S)$ laws may put some limitation on the type of PDFs that a particular intermittent field follows. Similarly, some of these $K(S)$ relationships may contribute insight as to the relevance of large eddy simulation parametrizations by providing constraints on the flow characteristics.

The role of anisotropy in interpreting the dynamics of turbulent flows is complex, including at larger R_V such as that encountered in the atmosphere (Lovejoy, Schertzer & Stanway 2001). For example, it is shown in Galtier (2023) that it affects in different ways the amplitude of the energy distribution and the spectral indices, so more work will be needed in that direction as well; we already know that, for anisotropic fluid flows in the presence of stratification, the skewness and kurtosis of velocity components can be direction-dependent (Bos, Liechtenstein & Schneider 2007; see also Homann *et al.* 2014 for the fast dynamo), and that anisotropic scaling laws can be developed phenomenologically and found observationally (Nazarenko & Schekochihin 2011; Bian & Li 2024).

When the velocity field is chaotic but not yet fully turbulent, and close to threshold for dynamo action, Sweet *et al.* (2001) identified a temporal bursty 'on–off' behavior of the dynamo-generated magnetic field which grows on average linearly with the control parameter, i.e. the distance in R_M from the threshold (see also Ponty *et al.* 2007; Alexakis & Ponty 2008, but these authors did not give indications on the behavior of the first few moments of the growing field). In Alexakis & Ponty (2008), the Lorentz force feedback on the flow is studied in detail with DNS ran for up to $10^5\tau_{nl}$ and for various P_M. They find that the Lorentz force strongly modifies the temporal evolution of the growing field through a control of the noise. We already know that the noise can alter the coefficients in a parabolic relation (Theodorsen, Garcia & Rypdal 2017; Losada *et al.* 2023), so we might be able to observe a change of scaling once we enter a turbulent saturation regime for the dynamo at higher Reynolds numbers, as we did for stratified flows (Pouquet *et al.* 2023). This is left for future work.

Acknowledgements

Y.P. thanks A. Miniussi for computing design assistance on the CUBBY code. The authors are grateful to the OPAL infrastructure from Université Côte d'Azur, the Université Côte d'Azur's Center for High-Performance Computing and to the national French computer facilities (GENCI) for providing resources and support. A.P. is thankful to Bob Ergun for his encouragement.

Editor Steve Tobias thanks the referees for their advice in evaluating this article.

Declaration of interests

The authors report no conflict of interest.

REFERENCES

ADHIKARI, S., SHAY, M.A., PARASHAR, T.N., PYAKUREL, P.S., MATTHAEUS, W., GODZIEBA, D., STAWARZ, J., EASTWOOD, J.P. & DAHLIN, J.T. 2020 Reconnection from a turbulence perspective. *Phys. Plasmas* **27** (4), 042305.

ALEXAKIS, A. & PONTY, Y. 2008 Effect of the Lorentz force on on-off dynamo intermittency. *Phys. Rev. E* **77** (5), 056308.

ASCHWANDEN, M.J. *et al.* 2016 25 years of self-organized criticality: solar and astrophysics. *Space Sci. Rev.* **198** (1-4), 47–166.

BERTIN, E. & CLUSEL, M. 2006 Generalized extreme value statistics and sum of correlated variables. *J. Phys. A* **39** (24), 7607–7619.

BIAN, N.H. & LI, G. 2024 Lagrangian perspectives on the small-scale structure of alfvénic turbulence and stochastic models for the dispersion of fluid particles and magnetic field lines in the solar wind. *Astrophys. J. Suppl.* **273** (1), 15.

BIRI, S., SCHARFFENBERG, M.G. & STAMMER, D. 2015 A probabilistic description of the mesoscale eddy field in the ocean. *J. Geophys. Res.* **120** (7), 4778–4802.

BOS, W., LIECHTENSTEIN, L. & SCHNEIDER, K. 2007 Small-scale intermittency in anisotropic turbulence. *Phys. Rev. E.* **67** (4), 046310.

BRADSHAW, Z., FARHAT, A. & GRUJIC, Z. 2019 An algebraic reduction of the scaling gap in the Navier–Stokes regularity problem. *Arch. Rat. Mech. Anal.* **231** (3), 1963–2005.

BRANDENBURG, A. & SUBRAMANIAN, K. 2005 Astrophysical magnetic fields and nonlinear dynamo theory. *Phys. Rep.* **417** (1), 1–209.

BUARIA, D., PUMIR, A. & BODENSCHATZ, E. 2022 Generation of intense dissipation in high Reynolds number turbulence. *Phil. Trans. A* **380** (2218), 20210088.

CAMPOREALE, E., SORRISO-VALVO, L., CALIFANO, F. & RETINÓ, A. 2018 Coherent structures and spectral energy transfer in turbulent plasma: a space-filter approach. *Phys. Rev. Lett.* **120**, 125101.

CHEN, C. 2016 Recent progress in astrophysical plasma turbulence from solar wind observations. *J. Plasma Phys.* **82** (6), 535820602.

ERGUN, R.E. *et al.* 2020 Observations of particle acceleration in magnetic reconnection-driven turbulence. *Astrophys. J.* **898** (2), 154.

FURNO, I. *et al.* 2015 Plasma turbulence, suprathermal ion dynamics and code validation on the basic plasma physics device torpex. *J. Plasma Phys.* **81** (3), 345810301. doi: 10.1017/S0022377815000161

GALTIER, S. 2023 Fast magneto-acoustic wave turbulence and the Iroshnikov–Kraichnan spectrum. *J. Plasma Phys.* **89** (2), 905890205.

GARCIA, O.E. 2012 Stochastic modeling of intermittent scrape-off layer plasma fluctuations. *Phys. Rev. Lett.* **108** (26), 265001.

GRAUER, R., KRUG, J. & MARIANI, C. 1994 Scaling of high-order structure functions in magnetohydrodynamic turbulence. *Phys. Lett. A* **195** (5-6), 335–338.

GUSZEJNOV, D., LAZANYI, N., BENCZE, A. & ZOLETNIK, S. 2013 On the effect of intermittency of turbulence on the parabolic relation between skewness and kurtosis in magnetized plasmas. *Phys. Plasmas* **20** (11), 112305.

VAN HAREN, H., CIMATORIBUS, A.A., CYR, F. & GOSTIAUX, L. 2016 Insights from a 3-D temperature sensors mooring on stratified ocean turbulence. *Geophys. Res. Lett.* **10** (1002/2016GL068032), 1–7.

HASSELMANN, K. 1962 On the non-linear energy transfer in a gravity-wave spectrum. Part 1. General theory. *J. Fluid Mech.* **12** (04), 481–500.

HOMANN, H., PONTY, Y., KRSTULOVIC, G. & GRAUER, R. 2014 Structures and lagrangian statistics of the Taylor–Green dynamo. *New J. Phys.* **16** (7), 075014.

HUGHES, C.W., THOMPSON, A.F. & WILSON, C. 2010 Identification of jets and mixing barriers from sea level and vorticity measurements using simple statistics. *Ocean Model.* **32** (1-2), 44–57.

IMAZIO, P.R., MININNI, P.D., GODOY, A., RIVABEN, N. & DÖRNBRACK, A. 2023 Not all clear air turbulence is kolmogorov – the fine-scale nature of atmospheric turbulence. *J. Geophys. Res.: Atmos.* **128** (2), e2022JD037491.

KOLMOGOROV, A.N. 1941 Dissipation of energy in locally isotropic turbulence. *Proc. R. Soc. Lond. A* **434**(1991), 15–17.

KRAICHNAN, R.H. 1967 Intermittency in the very small scales of turbulence. *Phys. Fluids* **10** (9), 2080–2082.

KROMMES, J.A. 2008 The remarkable similarity between the scaling of kurtosis with squared skewness for TORPEX density fluctuations and sea-surface temperature fluctuations. *Phys. Plasmas* **15** (3), 030703.

LABIT, B., FURNO, I., FASOLI, A., DIALLO, A., MÜLLER, S., PLYUSHCHEV, G., PODESTÀ, M. & POLI, F. 2007 Universal statistical properties of drift-interchange turbulence in TORPEX plasmas. *Phys. Rev. Lett.* **98** (25), 255002.

LENSCHOW, D., MANN, J. & KRISTENSEN, L. 1994 How long is long enough when measuring fluxes and other turbulence statistics? *J. Atmos. Ocean. Technol.* **11** (3), 661–673.

LOSADA, J.M., THEODORSEN, A. & GARCIA, O.E. 2023 Stochastic modeling of blob-like plasma filaments in the scrape-off layer: theoretical foundation. *Phys. Plasmas* **30** (4), 042518.

LOVEJOY, S., SCHERTZER, D. & STANWAY, J.D. 2001 Direct evidence of multifractal atmospheric cascades from planetary scales down to 1 km. *Phys. Rev. Lett.* **86** (22), 5200–5203.

MALLET, A., SCHEKOCHIHIN, A.A. & CHANDRAN, B.D. 2017 Disruption of alfvénic turbulence by magnetic reconnection in a collisionless plasma. *JPP* **466**, 1–22.

MARINO, R., FERACO, F., PRIMAVERA, L., PUMIR, A., POUQUET, A. & ROSENBERG, D. 2022 Turbulence generation by large-scale extreme drafts and the modulation of local energy dissipation in stably stratified geophysical flows. *Phys. Rev. Fluids* **7** (3), 033801.

MARINO, R. & SORRISO-VALVO, L. 2023 Scaling laws for the energy transfer in space plasma turbulence. *Phys. Rep.* **1006**, 1–144.

MATTHAEUS, W.H., WAN, M., SERVIDIO, S., GRECO, A., OSMAN, K.T., OUGHTON, S. & DMITRUK, P. 2015 Intermittency, nonlinear dynamics and dissipation in the solar wind and astrophysical plasmas. *Phil. Trans. R. Soc. A* **373** (2041), 20140154.

MENEGUZZI, M., POLITANO, H., POUQUET, A. & ZOLVER, M. 1996 A sparse-mode spectral method for the simulations of turbulent flows. *J. Comput. Phys.* **123** (1), 32–44.

MEZAOUI, H., HAMZA, A. & JAYACHANDRAN, P. 2014 Investigating high-latitude ionospheric turbulence using global positioning system data. *Geophys. Res. Lett.* **41** (19), 6570–6576.

MIRANDA, R.A., SCHELIN, A.B., CHIAN, A.C.-L. & FERREIRA, J.L. 2018 Non-Gaussianity and cross-scale coupling in interplanetary magnetic field turbulence during a rope-rope magnetic reconnection event. *Ann. Geophys.* **36** (2), 497–507.

NAZARENKO, S. & SCHEKOCHIHIN, S. 2011 Critical balance in magnetohydrodynamic, rotating and stratified turbulence: towards a universal scaling conjecture. *J. Fluid Mech.* **677**, 134–153.

PETOUKHOV, V., ELISEEV, A., KLEIN, R. & OESTERLE, H. 2008 On statistics of the free-troposphere synoptic component: an evaluation of skewnesses and mixed third-order moments contribution to the synoptic-scale dynamics and fluxes of heat and humidity. *Tellus* **60A**, 11–31.

POLITANO, H. & POUQUET, A. 1995 Model of intermittency in magnetohydrodynamic turbulence. *Phys. Rev. E* **52** (1), 636–641.

POLITANO, H., POUQUET, A. & SULEM, P.L. 1995 Current and vorticity dynamics in three–dimensional turbulence. *Phys. Plasmas* **2** (8), 2931–2939.

PONTY, Y., LAVAL, J., DUBRULLE, B., DAVIAUD, F. & PINTON, J.-F. 2007 Subcritical dynamo bifurcation in the Taylor–Green flow. *Phys. Rev. Lett.* **99** (22), 224501.

PONTY, Y., MININNI, P.D., MONTGOMERY, D., PINTON, J.-F., POLITANO, H. & POUQUET, A. 2005 Critical magnetic Reynolds number for dynamo action as a function of magnetic Prandtl number. *Phys. Rev. Lett.* **94** (16), 164502.

POUQUET, A., MARINO, R., POLITANO, H., PONTY, Y. & ROSENBERG, D. 2025 Intermittency in fluid and MHD turbulence analyzed through the prism of moment scaling predictions of multifractal models. *Nonlin. Proc. Geophys.* Under revision

POUQUET, A., ROSENBERG, D., MARINO, R. & MININNI, P. 2023 Intermittency scaling for mixing and dissipation in rotating stratified turbulence at the edge of instability. *Atmosphere* **14** (9), 01375.

RAFNER, J., GRUJIC, Z., BACH, C., BÆRENTZEN, J., GERVANG, B., JIA R.AND LEINWEBER, S. & MISZTAL, M.AND SHERSON, J. 2021 Geometry of turbulent dissipation and the Navier–Stokes regularity problem. *Sci. Rep.* **11** (1), 8824.

RINCON, F. 2019 Dynamo theories. *J. Plasma Phys.* **85** (4), 205850401. doi: 10.1017/S0022377819000539

SATTIN, F. *et al.* 2009 On the statistics of edge fluctuations: comparative study between various fusion devices. *Plasma Phys. Control. Fusion* **51** (5), 055013.

SCHEKOCHIHIN, A.A. 2022 MHD turbulence: a biased review. *J. Plasma Phys.* **88** (5), 155880501.

SHE, Z. & LÉVÊQUE, E. 1994 Universal scaling laws in fully developed turbulence. *Phys. Rev. Lett.* **72** (3), 336–339.

SLADKOMEDOVA, A., CZIEGLER, I., FIELD, A.R., SCHEKOCHIHIN, A.A. & IVANOV, P.G. 2023 Intermittency of density fluctuations and zonal-flow generation in MAST edge plasmas. *J. Plasma Phys.* **89** (6), 1–35.

SORRISO-VALVO, L., CARBONE, F., PERRI, S., GRECO, A., MARINO, R. & BRUNO, R. 2018 On the statistical properties of turbulent energy transfer rate in the inner heliosphere. *Solar Phys.* **293** (1), 10.

SURA, P. & SARDESHMUKH, P.D. 2008 A global view of Non-Gaussian SST variability. *J. Phys. Oceanogr.* **38** (3), 639–647.

SWEET, D., OTT, E., ANTONSEN, T.M., LATHROP, D.P. & FINN, J.M. 2001 Blowout bifurcations and the onset of magnetic dynamo action. *Phys. Plasmas* **8** (5), 1944–1952.

THEODORSEN, A., GARCIA, O. & RYPDAL, M. 2017 Statistical properties of a filtered Poisson process with additive random noise: distributions, correlations and moment estimation. *Phys. Scripta* **92** (5), 054002.

WAN, M., OUGHTON, S., SERVIDIO, S. & MATTHAEUS, W.H. 2010 On the accuracy of simulations of turbulence. *Phys. Plasmas* **17** (8), 082308.

WU, H., HUANG, S., WANG, X., YUAN, Z., HE, J. & YANG, L. 2023 Intermittency of magnetic discontinuities in the near-sun solar wind turbulence. *Astrophys. J. Lett.* **947** (2), L22.

YEUNG, P.K., ZHAI, X.M. & SREENIVASAN, K.R. 2015 Extreme events in computational turbulence. *Proc. Natl Acad. Sci.* **112** (41), 12633–12638.

ZHDANKIN, V., BOLDYREV, S. & MASON, J. 2017 Influence of a large-scale field on energy dissipation in magnetohydrodynamic turbulence. *Mon. Not. R. Astron. Soc.* **468** (4), 4025–4029.

ZIENICKE, E., POLITANO, H. & POUQUET, A. 1998 Variable intensity of Lagrangian chaos in the nonlinear dynamo problem. *Phys. Rev. Lett.* **81** (21), 4640–4643.